Geology, published online on 19 May 2015 as doi:10.1130/G36650.1

Giant Kiruna-type deposits form by efficient flotation of magmatic magnetite suspensions

Jaayke L. Knipping[1]*, Laura D. Bilenker[1], Adam C. Simon[1], Martin Reich[2], Fernando Barra[2], Artur P. Deditius[3], Craig Lundstrom[4], Ilya Bindeman[5], and Rodrigo Munizaga[6]

[1]Department of Earth and Environmental Sciences, University of Michigan, 1100 North University Avenue, Ann Arbor, Michigan 48109-1005, USA

[2]Department of Geology and Andean Geothermal Center of Excellence (CEGA), Universidad de Chile, Plaza Ercilla 803, Santiago 8320198, Chile

[3]School of Engineering and Information Technology, Murdoch University, 90 South Street, Murdoch, Western Australia 6150, Australia

[4]Department of Geology, University of Illinois, 605 East Springfield Avenue, Champaign, Illinois 61820, USA

[5]Department of Geological Sciences, University of Oregon, 1275 E 13th Avenue, Eugene, Oregon 97403-1272, USA

[6]Compañía Minera del Pacífico (CAP), Brasil N 1050, Vallenar, Región de Atacama 1610000, Chile

ABSTRACT

Kiruna-type iron oxide–apatite (IOA) deposits are an important source of Fe ore, and two radically different processes are being actively investigated for their origin. One hypothesis invokes direct crystallization of immiscible Fe-rich melt that separated from a parent silicate magma, while the other hypothesis invokes deposition of Fe-oxides from hydrothermal fluids of either magmatic or crustal origin. Here, we present a new model based on Fe and O stable isotopes and trace and major element geochemistry data of magnetite from the ~350 Mt Fe Los Colorados IOA deposit in the Chilean iron belt that merges these divergent processes into a single sequence of events that explains all characteristic features of these curious deposits. We propose that concentration of magnetite takes place by the preferred wetting of magnetite, followed by buoyant segregation of these early-formed magmatic magnetite-bubble pairs, which become a rising magnetite suspension that deposits massive magnetite in regional-scale transcurrent faults. Our data demonstrate an unambiguous magmatic origin, consistent with the namesake IOA analogue in the Kiruna district, Sweden. Further, our model explains the observed coexisting purely magmatic and hydrothermal-magmatic features and allows a genetic connection between Kiruna-type IOA and iron oxide–copper–gold deposits, contributing to a global understanding valuable to exploration efforts.

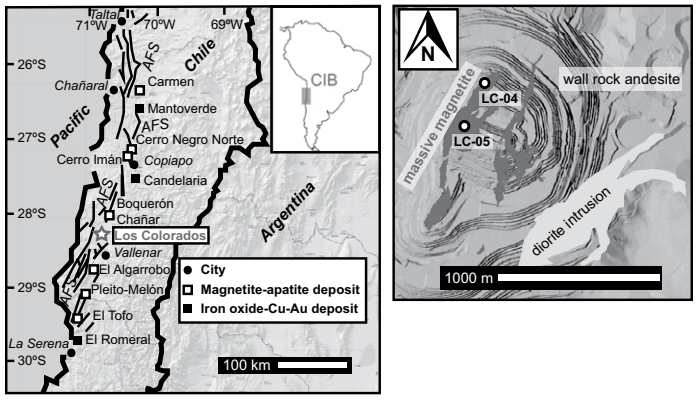

Figure 1. Map of Los Colorados within the Cretaceous Chilean iron belt (CIB). Right-hand image shows magnetite ore bodies, adjacent diorite intrusion, and location of investigated drill cores (LC-04, LC-05). AFS—Atacama fault system.

INTRODUCTION

The Los Colorados (LC) deposit, in the Cretaceous Chilean iron belt in the Coastal Cordillera of northern Chile (25–31°S) (Fig. 1), was formed during the breakup of Gondwana, which forced the Pacific margin into flat subduction (Chen et al., 2012). The inversion of extensional back-arc basins caused transcurrent crustal-scale fault zones (Atacama fault system), which host ~50 Fe iron oxide–apatite (IOA) deposits; seven each contain >100 Mt high-grade ore (Nyström and Henríquez, 1994). These deposits share characteristics with large IOA deposits in the giant Proterozoic Kiruna district (>100 Mt Fe) of Sweden (Nyström and Henríquez, 1994; Jonsson et al., 2013), including similar tectonic stress changes in a former back-arc setting (Allen et al., 2008). However, deposits in the Kiruna district have been disturbed by later alteration and metamorphism that complicate mineralogical and geochemical investigations. The origin of Kiruna-type IOA deposits remains controversial, and fundamentally different formation processes have been suggested. Several working hypotheses, including magmatic-hydrothermal replacement (Sillitoe and Burrows, 2002), hydrothermal precipitation in the sense of iron oxide–copper–gold (IOCG) deposits (Barton, 2014), and liquid immiscibility (Nyström and Henríquez, 1994; Naslund et al., 2002), have been invoked to explain, e.g., the vesiculated "magnetite lava flows" at the El Laco IOA deposit northeast of the Chilean iron belt (Park, 1961; Nyström and Henríquez, 1994). Iron ore at LC consists of massive magnetite (≤90% modal) in two kilometer-scale subparallel "dikes" (110 Ma), which are exposed along the strike of the southern segment of the Atacama fault system and associated with a diorite intrusion (108 Ma) (Pincheira et al., 1990) (Fig. 1). Magnetite crystals contain polycrystalline silicate and halite-bearing fluid inclusions (<5 μm). Coeval actinolite, clinopyroxene, and minor apatite are present, and the ore body lacks sodic and potassic alteration phases.

MAGMATIC STABLE ISOTOPE SIGNATURES AT LOS COLORADOS

We report stable Fe and O isotope pairs for 13 samples from two drill cores of the LC deposit (LC-04, LC-05), one representative sample from the extensively overprinted Fe-oxide deposit at Mineville, New York (USA) (Valley et al., 2011), and one from the Kiruna deposit, Sweden. Iron isotope values were obtained following the double-spike method of Millet et al. (2012). The resulting $\delta^{56}Fe_{mgt}$ values for LC magnetite range from 0.09‰ to 0.24‰ (average $\delta^{56}Fe_{mgt}$ [±2σ] = 0.17‰ ± 0.05‰) and $\delta^{18}O_{mgt}$ values range from 1.92‰ to 3.17‰ (average $\delta^{18}O_{mgt}$ [±2σ] = 2.60‰ ± 0.04‰) (Fig. 2; Item DR1 in the GSA Data Repository[1]). Iron and O isotope compositions of magnetite precipitated from a silicate melt or magmatic-hydrothermal aqueous fluid range from 0.06‰ to 0.5‰ and from 1.0‰ to 4.0‰,

*E-mail: jaaykek@umich.edu

[1]GSA Data Repository item 2015206, Fe and O isotope data (DR1), EPMA data (DR2) and model calculations (DR3), is available online at www.geosociety.org/pubs/ft2015.htm, or on request from editing@geosociety.org or Documents Secretary, GSA, P.O. Box 9140, Boulder, CO 80301, USA.

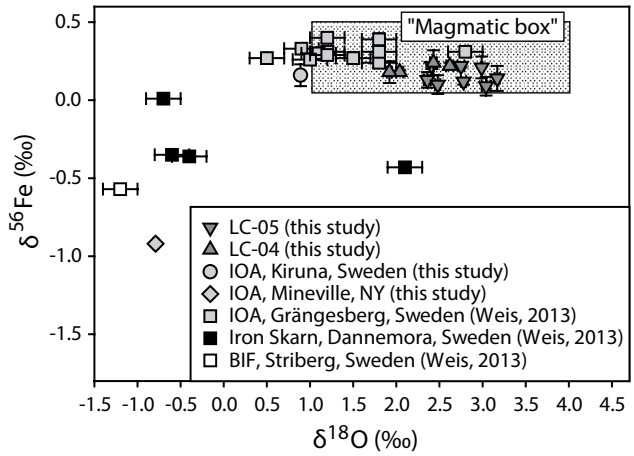

Figure 2. $\delta^{18}O$ versus $\delta^{56}Fe$ isotope values of magnetite. Box shows range for magmatic magnetite (Heimann et al., 2008; Taylor, 1967; Weis, 2013), within which Los Colorados (LC) data distinctively plot. Data of a skarn, banded iron formation (BIF), and iron oxide–apatite (IOA) deposits in Sweden, and altered Mineville IOA deposit (New York, USA), are plotted for comparison. Non-magmatic deposits (skarn and BIF) plot outside of magmatic box, reflecting lighter Fe and O isotopic composition. Uncertainties are ±2σ and may be smaller than symbol size.

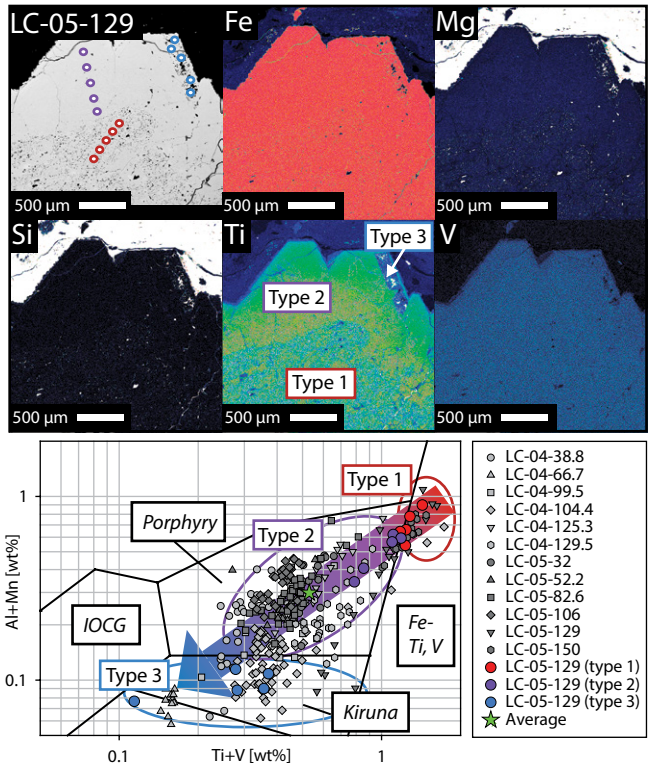

Figure 3. Elemental maps of Los Colorados magnetite, and magnetite chemistry plotted on discriminant diagram of Dupuis and Beaudoin (2011) and Nadoll et al. (2014). Elemental maps reveal core-to-rim zonation from igneous to magmatic-hydrothermal magnetite, and (Ti + V) versus (Al + Mn) diagram shows distribution of Los Colorados samples from high to low values. Colored circles in backscattered electron image represent positions of the measured data points. Star is average of all Los Colorados magnetites. IOCG—iron oxide–copper–gold.

respectively, based on analyses of natural samples of known igneous origin (Heimann et al., 2008; Taylor, 1967). The isotopic signature of magnetite at LC overlaps these established magmatic values. The data also overlap the Fe and O isotope signature of magnetite from the Kiruna district (Jonsson et al., 2013; Weis, 2013), and eliminate a purely low-temperature (*T*) hydrothermal origin for the Fe ore. In contrast, data for magnetite from Mineville demonstrate that hydrothermal alteration–related mineralization (Valley et al., 2011) shifts $\delta^{56}Fe_{mgt}$ and $\delta^{18}O_{mgt}$ to lower values (Fig. 2).

MAGMATIC TO HYDROTHERMAL GEOCHEMICAL ZONING OF MAGNETITE

To distinguish between purely igneous and magmatic-hydrothermal signatures that are merged as "magmatic" in the previous section, high-resolution trace element analyses were performed on individual magnetite grains. Electron probe microanalyses (Item DR2) of most magnetite grains from the center of the western dike (LC-05) and its border zone (LC-04) indicate a high-*T* magmatic origin (porphyry type) according to discrimination diagrams ([Ti + V] vs. [Al + Mn]) of Dupuis and Beaudoin (2011) and Nadoll et al. (2014) (Fig. 3). However, some magnetite grains are zoned (Fig. 3) with euhedral cores rich in silicate inclusions (type 1) within a less porous magnetite matrix (type 2), which can be surrounded by a third generation of porous magnetite (type 3). The compositions of the magnetite cores (type 1) are consistent with Ti-rich magnetite in nelsonites (Fe-Ti, V field in Fig. 3), which are thought to form by purely magmatic processes, while type 2 magnetite has a high-*T* magmatic-hydrothermal fluid signature (porphyry field). Only samples distal from the dike center or distal from the grain cores (i.e., late growth zones) have (Ti + V) and (Al + Mn) as low as expected for magnetite of the Kiruna field (cf. Dupuis and Beaudoin, 2011) in Figure 3 (type 3 magnetite). The chemical patterns are therefore best interpreted to reflect a change from purely magmatic to magmatic-hydrothermal conditions during crystallization of the LC magnetite.

A NEW MODEL: MAGNETITE SEGREGATION, SUSPENSION, AND TRANSPORT

The data presented here indicate that LC magnetite records a transition from purely magmatic conditions (type 1) to high-*T* magmatic-hydrothermal conditions (type 2) with decreasing *T* (type 3). This compositional change suggests that the formation of the LC magnetite ore resulted from a sequence of events involving a melt and a magmatic-hydrothermal fluid. We propose the following model to explain this process:

(1) In hydrous, oxidized arc magmas, magnetite is the first liquidus phase at 200 MPa (Martel et al., 1999), which facilitates H_2O saturation (Hurwitz and Navon, 1994). To reduce surface energies, bubbles nucleate on crystal surfaces (heterogeneous bubble nucleation). However, fluids exclusively attach to magnetite microlites due to larger wetting angles between fluids and oxides (45°–50°) compared to silicates (5°–25°) (Gualda and Ghiorso, 2007; Edmonds et al., 2014) (Fig. 4A).

(2) Bubble-magnetite pairs (i.e., fluid bubbles attached to magnetite microlites) rise (Fig. 4B) when the buoyancy force $F^{buoyancy} > 0$ (Gualda and Ghiorso, 2007), which can be estimated by:

$$F^{buoyancy} = \left(V_{bubble} \cdot \Delta\rho_{bubble} - V_{mgt} \cdot \Delta\rho_{mgt}\right) \cdot g. \quad (1)$$

Here, V_{bubble} and V_{mgt} are the volumes of bubble and magnetite, respectively, g is gravitational force, and Δρ is the density difference between melt and bubble ($\Delta\rho_{bubble}$) or between magnetite and melt ($\Delta\rho_{mgt}$). A magnetite-bubble pair will not ascend when $F^{buoyancy} \leq 0$. Thus, the critical ratio of V_{bubble}/V_{mgt} at which these aggregates will ascend in the magma chamber can be calculated by:

$$\frac{V_{bubble}}{V_{mgt}} = \frac{\rho_{mgt}}{\rho_{bubble}}. \quad (2)$$

We assume ρ_{mgt} = 5.20 g/cm³ and ρ_{melt} = 2.27 g/cm³ for a hydrous (6 wt% H_2O) andesite (cf. Ochs and Lange, 1999) at 1000°C and 200 MPa. Our proposed model uses a fluid with a bulk salinity of 35 wt%

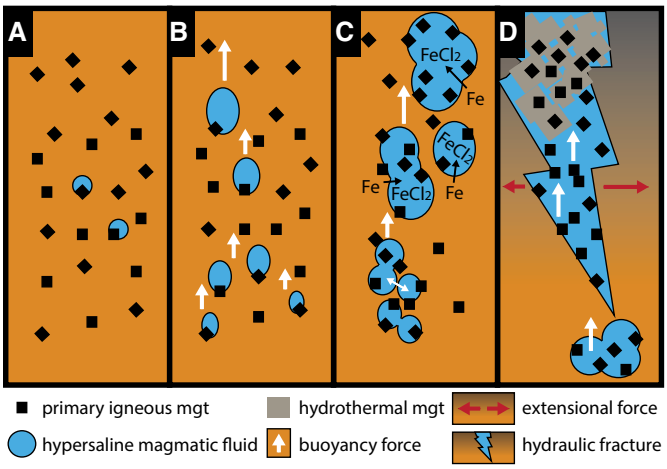

Figure 4. Model proposed showing preferred bubble nucleation on magnetite (mgt) microlites crystallized from silicate melt (orange) (A), ascent of bubble-magnetite pairs due to positive $F^{buoyancy}$ (B), further ascent, growth, coalescence, and accumulation of primary magnetite as well as scavenging of Fe into the high-salinity fluids (C), formation of hydraulic fractures (due to tectonic stress changes) allowing fast, efficient segregation of magnetite-rich fluid (D), and eventual growth of hydrothermal magnetite during progressive cooling. Panels represent scenarios becoming shallower from A to D. Color change in D implies increasing crystallinity.

$NaCl_{eq}$ based on the presence of euhedral halite in our magnetite-hosted fluid inclusions (Bodnar and Vityk, 1994). This fluid further contains 7.2 wt% Fe based on published magnetite solubility data (Simon et al., 2004). Using an equation of state for 1000 °C and 200 MPa (Pitzer and Sterner, 1995; Driesner, 2007) and the aforementioned fluid chemistry, ρ_{bubble} is 0.51 g/cm^3. These parameters allow $F^{buoyancy} > 0$ as long as magnetite composes <37 vol% of the magnetite-bubble aggregate. Experimental evidence for flotation of ore minerals by such a process is reported by Matveev and Ballhaus (2002) and Mungall et al. (2015).

(3) These aggregates grow, coalesce, and sweep up other magnetite microlites during ascent, becoming a rising suspension with up to 37 vol% (65 wt%) magnetite (Fig. 4C). Once magnetite microlites are enclosed within the suspension, their chemistry will be controlled by the aqueous fluid and reflect partitioning of elements between melt, aqueous fluid, and magnetite. Hence, the concentration of fluid-immobile elements such as Ti, V, Al, and Mn, among others, should decrease in magnetite that grows from the aqueous fluid component of the suspension, and the magnetite chemistry should become magmatic-hydrothermal (type 2 magnetite). Published experimental data demonstrate that Cl-bearing aqueous fluids can scavenge up to several weight percent Fe from the melt as $FeCl_2$ (Simon et al., 2004; Bell and Simon, 2011) (Fig. 4C), allowing for type 2 and type 3 magnetite to grow during ascent and cooling (Fig. 4D). Abundant Cl in the melt can be explained by seawater recycling of the subducted slab (Philippot et al., 1998). Chlorine-bearing aqueous brine also effectively scavenges P, among other fluid-compatible elements, from silicate melt, with reported brine-melt partition coefficients for P ranging from 2 to 6 (Zajacz et al., 2008). The magnetite suspension ascends through the melt-dominated magma, owing to increasing V_{bubble} and thus decreasing ρ_{bubble} during ascent (decompression), and forms larger magnetite-suspension pockets (Fig. 4C).

(4) Instead of forming just magnetite-rich enclaves as described by Edmonds et al. (2014), we propose that tectonic stress changes cause, in the case of LC, an efficient ascent of the magnetite suspension. A sudden destabilization of the magma body results in rapid transport (5–20 m/s) through hydraulic fractures in a ductile crystal-mush regime (Hautmann et al., 2014), wherein high-flux permeable channels become well developed with increasing crystallinity (cf. Hersum et al., 2005). This is a plausible, repeatable scenario for the formation of the LC deposit, due to the tectonic activity along the Atacama fault system during the Early Cretaceous, which also explains the spatial relationship between the Chilean iron belt and the Atacama fault system. Finally, the magnetite suspension(s) accumulate in large crustal faults owing to decreasing pressure and T, trapping additional phases such as brine and silicates as inclusions (Fig. 4D). Euhedral actinolite, apatite, and clinopyroxene may co-crystallize, similar to observations in decompression experiments for chromite deposits (Matveev and Ballhaus, 2002).

Incorporation of primary (type 1) magnetite into the exsolved magmatic-hydrothermal aqueous fluid phase would not only explain the detected geochemical signature, but would also decrease the magma volume required to produce the ~350 Mt Fe ore deposit at LC. For instance, for a hydrous (6 wt% H_2O) andesitic magma (ρ = 2.27 g/cm^3), the addition of 20 wt% primary magnetite into the fluid phase (mass proportion of magnetite in the suspension) would decrease the required magma chamber size from >150 to 50 km^3 when 20% degassing and a 50% depositional efficiency of dissolved Fe are assumed. In this case, the fluid that ascends after formation of the LC deposit retains half of its original dissolved Fe. Notably, the parental magma loses only 0.7 wt% FeO (see Item DR3 for model calculations).

A GENETIC LINK BETWEEN IOA AND IOCG DEPOSITS?

Our proposed magnetite suspension model accounts for the observed combination of primary igneous (type 1) and secondary high-T hydrothermal magnetite (type 2), and can also explain the lack of K and Na alteration at LC and potentially a genetic link between IOA and IOCG deposits. Simon et al. (2004) reported that the Fe concentration of a Cl-rich aqueous fluid decreases slightly during decompression, while concentrations of Na and K strongly increase, allowing for magnetite precipitation without simultaneous Na and K mineralization. However, owing to retrograde solubility of metals such as Fe, Cu, and Au (Williams-Jones and Migdisov, 2014; Hurtig and Williams-Jones, 2014), the magmatic-hydrothermal fluid that precipitates magnetite will continue transporting significant amounts of dissolved Fe (plus Cu, Au) after IOA deposition. Further ascent and cooling promotes the precipitation of Cu-sulfides at T < 420 °C and at shallow levels within the crust, as observed for IOCG deposits. This is consistent with the proposed model in which IOA deposits represent the deeper roots of IOCG systems (e.g., Sillitoe, 2003), and may therefore be a step toward a systematic formation model for IOCG deposits.

CONCLUSION

The Chilean iron belt experienced an amalgamation of several factors including: (1) the formation of a Cl-rich hydrous mafic magma due to recycling of seawater during subduction; (2) crustal thinning in an extensional back-arc setting, allowing magma ascent into the shallow crust; and (3) a stress change during the Early Cretaceous that produced crustal-scale faults (Atacama fault system) to serve as conduits for magnetite-fluid suspensions. Our new magnetite-suspension model for the formation of Kiruna-type IOA deposits is supported by stable Fe and O isotope signatures and the contrasting magnetite geochemistry between silicate inclusion–rich igneous cores and the surrounding magmatic-hydrothermal magnetite matrix. The observed trend from high to low (Ti + V) and (Al + Mn) values (Fig. 3) can be explained by cooling magmatic-hydrothermal fluids because these elements become increasingly incompatible in magnetite and aqueous fluid at lower T. Eventually, further ascent and cooling reduces the ability of the fluid to maintain high concentrations of dissolved Fe and other elements (e.g., Cu, Au), which promotes the precipitation of Cu-sulfides and Fe-oxides at shallower levels than IOA deposits, supporting a genetic link between IOA and IOCG deposits. Lastly, it is plausible that a magnetite-fluid suspension vented to the surface could have produced the strongly vesiculated magnetite "lava flows" observed at El Laco, Chile (Park, 1961), with magnetite trace element patterns guiding researchers to a high-T magmatic-hydrothermal origin (Dare et al., 2014).

ACKNOWLEDGMENTS

We thank F. Pirajno, H.R Naslund, and V.R. Troll for helpful reviews. Simon and Reich thank Steve Kesler, who suggested this collaborative project. Knipping acknowledges a German Academic Exchange Service (DAAD) Ph.D. grant, and Bilenker acknowledges funding from the Society of Economic Geologists and the University of Michigan Rackham Graduate School. Simon acknowledges funding from U.S. National Science Foundation grants EAR-1250239 and EAR-1264537. Barra and Reich acknowledge funding from Fondecyt grant 1140780, funding from Millennium Science Initiative grant "Nucleus for Metal Tracing Along Subduction" (NC130065), and FONDAP grant 15090013. We thank M. Lagos and CAP for allowing access to the LC deposit, and the scientific and technical assistance of M. Roberts at the University of Western Australia.

REFERENCES CITED

Allen, R.L., Lundstrom, I., Ripa, M., and Christofferson, H., 2008, Facies analysis of a 1.9 Ga, continental margin, back-arc, felsic caldera province with diverse Zn-Pb-Ag-(Cu-Au) sulfide and Fe oxide deposits, Bergslagen region, Sweden: Economic Geology and the Bulletin of the Society of Economic Geologists, v. 91, p. 979–1008, doi:10.2113/gsecongeo.91.6.979.

Barton, M.D., 2014, Iron oxide(–Cu–Au–REE–P–Ag–U–Co) systems, *in* Scott, S.D., ed., Treatise on Geochemistry (second edition, volume 13): Amsterdam, Elsevier, p. 515–541.

Bell, A., and Simon, A.C., 2011, Evidence for the alteration of the $Fe^{3+}/\Sigma Fe$ of silicate melt caused by the degassing of chlorine-bearing aqueous volatiles: Geology, v. 39, p. 499–502, doi:10.1130/G31828.1.

Bodnar, R.J., and Vityk, M.O., 1994, Interpretation of microthermometric data of H_2O-NaCl fluid inclusions, *in* De Vivo, B., and Frezzotti, M.L., eds., Fluid Inclusions in Minerals: Methods and Applications: Blacksburg, Virginia, Virginia Tech, p. 117–130.

Chen, H., Cooke, D.R., and Baker, M.J., 2012, Mesozoic iron oxide copper-gold mineralization in the central Andes and the Gondwana Supercontinent breakup: Economic Geology and the Bulletin of the Society of Economic Geologists, v. 108, p. 37–44, doi:10.2113/econgeo.108.1.37.

Dare, S.A.S., Barnes, S.-J., and Beaudoin, G., 2014, Did the massive magnetite "lava flows" of El Laco (Chile) form by magmatic or hydrothermal processes? New constraints from magnetite composition by LA-ICP-MS: Mineralium Deposita, doi:10.1007/s00126-014-0560-1.

Driesner, T., 2007, The system H_2O–NaCl. Part II: Correlations for molar volume, enthalpy, and isobaric heat capacity from 0 to 1000 °C, 1 to 5000 bar, and 0 to 1 X_{NaCl}: Geochimica et Cosmochimica Acta, v. 71, p. 4902–4919, doi:10.1016/j.gca.2007.05.026.

Dupuis, C., and Beaudoin, G., 2011, Discriminant diagrams for iron oxide trace element fingerprinting of mineral deposit types: Mineralium Deposita, v. 46, p. 319–335, doi:10.1007/s00126-011-0334-y.

Edmonds, M., Brett, A., Herd, R.A., Humphreys, M.C.S., and Woods, A., 2014, Magnetite-bubble aggregates at mixing interfaces in andesite magma bodies, *in* Zellmer, G.F., et al., eds., The Role of Volatiles in the Genesis, Evolution and Eruption of Arc Magmas: Geological Society of London Special Publication 410, p. 95–121, doi:10.1144/SP410.7.

Gualda, G.A.R., and Ghiorso, M.S., 2007, Magnetite scavenging and the buoyancy of bubbles in magmas. Part 2: Energetics of crystal-bubble attachment in magmas: Contributions to Mineralogy and Petrology, v. 154, p. 479–490, doi:10.1007/s00410-007-0206-8.

Hautmann, S., Witham, F., Christopher, T., Cole, P., Linde, A.T., Sacks, S., and Sparks, S.J., 2014, Strain field analysis on Montserrat (W.I.) as tool for assessing permeable flow paths in the magmatic system of Soufriere Hills Volcano: Geochemistry Geophysics Geosystems, v. 15, p. 676–690, doi: 10.1002/2013GC005087.

Heimann, A., Beard, B.L., and Johnson, C.M., 2008, The role of volatile exsolution and subsolidus fluid/rock interactions in producing high $^{56}Fe/^{54}Fe$ ratios in siliceous igneous rocks: Geochimica et Cosmochimica Acta, v. 72, p. 4379–4396, doi:10.1016/j.gca.2008.06.009.

Hersum, T., Hilpert, M., and Marsh, B., 2005, Permeability and melt flow in simulated and natural partially molten basaltic magmas: Earth and Planetary Science Letters, v. 237, p. 798–814, doi:10.1016/j.epsl.2005.07.008.

Hurtig, N.C., and Williams-Jones, A.E., 2014, An experimental study of the transport of gold through hydration of AuCl in aqueous vapour and vapour-like fluids: Geochimica et Cosmochimica Acta, v. 127, p. 305–325, doi:10.1016/j.gca.2013.11.029.

Hurwitz, S., and Navon, O., 1994, Bubble nucleation in rhyolitic melts: Experiments at high pressure, temperature, and water content: Earth and Planetary Science Letters, v. 122, p. 267–280, doi:10.1016/0012-821X(94)90001-9.

Jonsson, E., Troll, V.R., Hoegdahl, K., Harris, C., Weis, F., Nilsson, K.P., and Skelton, A., 2013, Magmatic origin of giant 'Kiruna-type' apatite-iron-oxide ores in Central Sweden: Nature Scientific Reports, v. 3, p. 1644–1652, doi:10.1038/srep01644.

Martel, C., Pichavent, M., Holtz, F., and Scaillet, B., 1999, Effects of f_{O_2} and H_2O on andesite phase relations between 2 and 4 kbar: Journal of Geophysical Research, v. 104, p. 29,453–29,470, doi:10.1029/1999JB900191.

Matveev, S., and Ballhaus, C., 2002, Role of water in the origin of podiform chromitite deposits: Earth and Planetary Science Letters, v. 203, p. 235–243, doi:10.1016/S0012-821X(02)00860-9.

Millet, M., Baker, J., and Payne, C., 2012, Ultra-precise stable Fe isotope measurements by high-resolution multi-collector inductively coupled plasma mass spectrometry with a ^{57}Fe-^{58}Fe double spike: Chemical Geology, v. 304–305, p. 18–25, doi:10.1016/j.chemgeo.2012.01.021.

Mungall, J.E., Brenan, J.M., Godel, B., and Gaillard, F., 2015, Transport of metals and sulphur in magmas by flotation of sulphide melt on vapour bubbles: Nature Geoscience, v. 8, p. 216–219, doi:10.1038/ngeo2373.

Nadoll, P., Angerer, T., Mauk, J.L., French, D., and Walshe, J., 2014, The chemistry of hydrothermal magnetite: A review: Ore Geology Reviews, v. 61, p. 1–32, doi:10.1016/j.oregeorev.2013.12.013.

Naslund, H.R., Henriquez, F., Nystroem, J.O., Vivallo, W., and Dobbs, F.M., 2002, Magmatic iron ores and associated mineralisation: Examples from the Chilean high Andes and coastal Cordillera, *in* Porter, T.M., ed., Hydrothermal Iron Oxide Copper-Gold and Related Deposits: A Global Perspective: Adelaide, Australia, PGC Publishing, v. 2, p. 207–226.

Nyström, J.O., and Henríquez, F., 1994, Magmatic features of iron ores of the Kiruna type in Chile and Sweden: Ore textures and magnetite geochemistry: Economic Geology and the Bulletin of the Society of Economic Geologists, v. 89, p. 820–839, doi:10.2113/gsecongeo.89.4.820.

Ochs, F.A., and Lange, R.A., 1999, The density of hydrous magmatic liquids: Science, v. 283, p. 1314–1317, doi:10.1126/science.283.5406.1314.

Park, C.F., Jr., 1961, A magnetite "flow" in northern Chile: Economic Geology and the Bulletin of the Society of Economic Geologists, v. 56, p. 431–436, doi:10.2113/gsecongeo.56.2.431.

Philippot, P., Agrinier, P., and Scambelluri, M., 1998, Chlorine cycling during subduction of altered oceanic crust: Earth and Planetary Science Letters, v. 161, p. 33–44, doi:10.1016/S0012-821X(98)00134-4.

Pincheira, M., Thiele, R., and Fontbote, L., 1990 Tectonic transpression along the southern segment of the Atacam Fault-Zone, Chile, *in* Proceedings, Symposium International "Géodynamique Andine", Grenoble, 15–17 May (Colloques et Seminaires): Paris, ORSTOM, p. 133–136.

Pitzer, K.S., and Sterner, S.M., 1995, Equations of state valid continuously from zero to extreme pressures with H_2O and CO_2 as examples: International Journal of Thermophysics, v. 16, p. 511–518, doi:10.1007/BF01441917.

Sillitoe, R.H., 2003, Iron oxide-copper-gold deposits: An Andean view: Mineralium Deposita, v. 38, p. 787–812, doi:10.1007/s00126-003-0379-7.

Sillitoe, R.H., and Burrows, D.R., 2002, New field evidence bearing on the origin of the El Laco magnetite deposit, northern Chile: Economic Geology and the Bulletin of the Society of Economic Geologists, v. 97, p. 1101–1109, doi:10.2113/gsecongeo.97.5.1101.

Simon, A.C., Pettke, T., Candela, P.A., Piccoli, P.M., and Heinrich, A.H., 2004, Magnetite solubility and iron transport in magmatic-hydrothermal environments: Geochimica et Cosmochimica Acta, v. 68, p. 4905–4914, doi: 10.1016/j.gca.2004.05.033.

Taylor, H.P., Jr., 1967, Oxygen isotope studies of hydrothermal mineral deposits, *in* Barnes, H.L., ed., Geochemistry of Hydrothermal Ore Deposits (first edition): New York, Holt, Rinehart and Winston, p. 109–142.

Valley, P.M., Hanchar, J.M., and Whitehouse, M.J., 2011, New insights on the evolution of the Lyon Mountain Granite and associated Kiruna-type magnetite-apatite deposits, Adirondack Mountains, New York State: Geosphere, v. 7, p. 357–389, doi:10.1130/GES00624.1.

Weis, F., 2013, Oxygen and iron isotope systematics of the Grängesberg mining district (GMD), central Sweden [M.S. thesis]: Uppsala, Sweden, Uppsala University, 83 p.

Williams-Jones, A.E., and Migdisov, A.A., 2014, Experimental constraints and deposition of metals in ore-forming hydrothermal systems, *in* Kelley, K.D., and Golden, H.C., eds., Building Exploration Capability for the 21st Century: Society of Economic Geologists Special Publication 18, p. 77–98.

Zajacz, Z., Halter, W.E., Pettke, T., and Guillong, M., 2008, Determination of fluid/melt partition coefficients by LA-ICPMS analysis of co-existing fluid and silicate melt inclusions: Controls on element partitioning: Geochimica et Cosmochimica Acta, v. 72, p. 2169–2197, doi:10.1016/j.gca.2008.01.034.

Manuscript received 23 January 2015
Revised manuscript received 16 April 2015
Manuscript accepted 18 April 2015

Printed in USA

Geology

Giant Kiruna-type deposits form by efficient flotation of magmatic magnetite suspensions

Jaayke L. Knipping, Laura D. Bilenker, Adam C. Simon, Martin Reich, Fernando Barra, Artur P. Deditius, Craig Lundstrom, Ilya Bindeman and Rodrigo Munizaga

Geology published online 19 May 2015;
doi: 10.1130/G36650.1